# Contribution of Mn content on the pressure dose properties

# Prispevek vpliva deleža Mn na lastnosti tlačnih doz

Jožef Medved[1], Tomaž Godicelj[2], Stanislav Kores[1], Primož Mrvar[1] & Maja Vončina[1,*]

[1]University of Ljubljana, Faculty of Material Science and Engineering, Department of Materials and Metallurgy, Aškerčeva 12, SI-1000 Ljubljana, Slovenia
[2]Talum d.d. Kidričevo, Tovarniška cesta 10, 2325 Kidričevo, Slovenia

*Corresponding author. E-mail: maja.voncina@omm.ntf.uni-lj.si

**Received:** May 28, 2012 **Accepted:** July 17, 2012

**Abstract:** For the pressure dose manufacture electrolytic aluminium and its alloys are used. With the purpose of improvement of the material properties and production rationalization, the optimal composition of the alloy must be achieved to reach good formability and mechanical properties with the best exploitation of the material.

The aim of this work was to analyse the properties of three alloys according the AA standard: 1050, 3002 and 3003 which are used in dose production. The investigation was made using computer simulation of phase equilibrium with Thermo-Calc program, optic and electron microscopy and technological testing. The Mn content in mentioned alloys influences the phase equilibrium as the content of the phases on base of Mn increases, increases the strength properties and raises the recrystallization threshold. Inclusions are at the longitudinal courses always longitudinal distributed (course of the impact extrusion) and of polyedric shape; on the bottom of the pressure dose (Pos.1), the inclusions can be found in bigger heaps. The results show that the hardness, deformation pressure and crack pressure increase with the increasing Mn content in the alloy.

**Izvleček:** Za izdelavo tlačnih doz se uporablja elektrolizni aluminij in njegove zlitine. Za izboljšanje lastnosti materiala in racionalizacije izdelave je treba zagotoviti optimalno sestavo zlitine tako, da bi dosegli dobre preoblikovalne in mehanske lastnosti ob čim manjši potrebni količini materiala.

*Preliminary notes*

Namen dela je bila analiza lastnosti treh zlitin po AA-standardih 1050, 3002 in 3003, ki se uporabljajo za izdelavo tlačnih doz. Preiskave zlitin so obsegale računalniško simulacijo faznih ravnotežij s programom Thermo-Calc, optično in elektronsko mikroskopijo ter tehnološke preizkuse. Delež Mn v obravnavanih zlitinah vpliva na fazno ravnotežje s povečanjem deleža faz na osnovi Mn, vpliva na povišanje trdnostnih lastnosti in rekristalizacijskega praga. Vključki so pri vzdolžnih smereh vedno vzdolžno razporejeni (smer protismernega stiskanja) ter poliedrične oblike, na dnu tlačnih doz (Poz.1) pa se vključki nahajajo v večjih skupkih. Rezultati so pokazali, da se trdota, deformacijski tlak ter razpočni tlak povečujejo z naraščajočo koncentracijo Mn v zlitini.

**Key words:** Al-Mn alloys, slugs, thermodynamics, mechanical properties
**Ključne besede:** Al-Mn zlitine, rondelice, termodinamika, mehanske lastnosti

## Introduction

AA 3XXX aluminium alloys find wide applications in the transportation, food, beverage and packaging industries. In these applications, control of the plastic anisotropy of the sheet is of great importance in order to ensure the formability of the final product and to reduce the waste of the material resulting from earing behaviour.[1] Conventionally, aluminium sheet is mainly produced by the direct chill (DC) cast technology. Continuous cast (CC) technology, a new technology, however provides both energy and economic savings while reducing environmental emissions that are more and more urgent issues in today's environment. Compared with DC cast technology, CC technology also takes advantage of high productivity.[2, 3]

Al-Mn alloys, known also as AA 3XXX series, distinguish good formability, corrosion resistance, good weldability and relatively good mechanical properties which make them very wanted alloys.[4] It is often used in a shape of plates and lamellas; they can be extruded or forged whereas their uses are limited.[5]

Slugs are used for the production of aluminium packaging tubes with or without membrane and for aerosol cans. Slugs are round, with or without a hole, surface treatment is tumbled or sandblasted, they can be flat or domed. Once punched, the slugs must go through an annealing process. Slugs and discs are produced from continuously cast and rolled narrow strip. The surface of the slugs must be smooth without obvious cracks.[6]

The type, size and distribution of dispersoids formed during solidification and cooling and during the homogenization process is of great importance.[7, 9] It has strong influences on the deformation behaviour, recrystallization behaviour and mechanical properties of non-heat-treatable 3xxx aluminium alloys. A better understanding of the precipitation behaviour of dispersoids is crucial to the optimization of the chemical compositions, homogenization processes and mechanical properties of the alloys. During annealing at 450 °C, two types of dispersoids precipitate in the alloy. They were identified as a thin elongated $Al_{12}Mn$ phase with a body centred cubic (bcc) structure and an equiaxed plate-shaped or needle shaped[5] $Al_7Mn$ phase with an orthorhombic structure. Both $Al_{12}Mn$ and orthorhombic $Al_7Mn$ dispersoids precipitate in binary 3003 alloy during annealing at temperatures lower than 550 °C. Since both phases are metastable, during annealing at higher temperatures, $Al_6Mn$ dispersoids precipitate as a stable phase. When there were trace levels of Fe and Si impurities in 3009 alloy, in addition to $Al_{12}Mn$ phase, hexagonal α-Al(Mn,Fe)Si phase[8] or plane cubic α-AlMnSi phase[9, 10] was found to precipitate in the alloy. The addition of alloying elements in 3XXX alloys has strong influence on the precipitation behaviour. Fe and Si greatly decrease the solubility of Mn in solid solution and accelerate the precipitation rate. Addition of Cu can also enhance the decomposition of the supersaturated solid solution. Fe favours the precipitation of $Al_6(Fe,Mn)$,[11] while Si favours the precipitation of cubic α-phase, $Al_{12}Mn_3Si$ or $Al_{12}(Fe,Mn)_3Si$ (when Fe is also present) in the alloy. α-Al(Mn,Fe)Si dispersoid, which is considered to be incoherent with the matrix, is a very important phase in 3xxx alloys.[12, 13]

## Materials and methods

As an entry material for the production of pressure dose, the slugs of 52.7 mm diameter and 8.6 mm of thickness were used. Three series of pressure doses were made from three various alloys: 1050, 3002 and 3003.

The production process of pressure dose is composed from seven following steps (Figure 1):
*(1) impact extrusion → (2) annealing* (280 °C) → *(3) interior protection* (140 °C) → *(4) drying of base colour* (200 °C) → *(5) printing → (6) drying of lacquer* (170 °C) → *(7) forming of cupola*

After each of these seven steps, five specimens were taken for further investigations. After the sampling, the specimens were systematically marked.

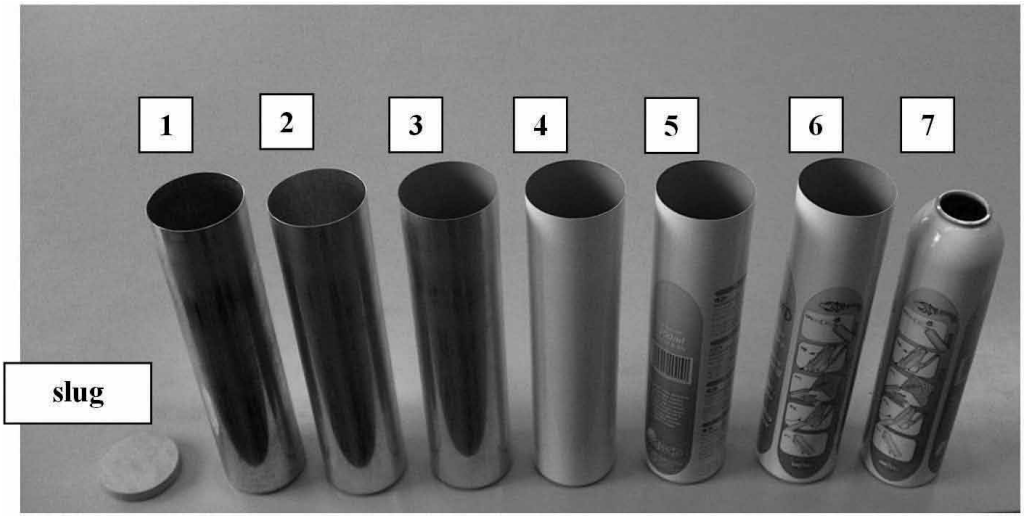


**Figure 1.** Specimens from the production process of pressure dose

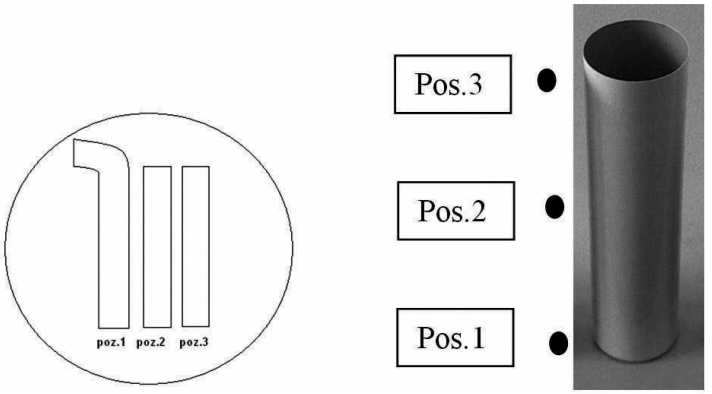


**Figure 2.** Sampling from the pressure dose

For each composition, the chemical analysis and computer simulation of thermodynamic equilibrium solidification with determination of equilibrium phase composition at room temperature using Thermo-Calc program and database COST507 were made.

**Sample preparation for the microscopy**

The samples for the microstructure analysis were taken from three places (samples from 1−7): from the bottom longitudinal to the forming course, at the place where the crossing of bottom to the wall was captured (pos.1), 1 cm from the top in a transversal course (pos.3) and longitudinal course (pos.2) according to the course of forming (Figure 2). Sample 0 represents the microstructure of a slug.

Optic microscope OLYMPUS BX61 equipped with video camera DP70 and analySIS 5.0 program was used for the microstructure analysis and the scanning electron microscope JEOL 5610 with EDS electron microanalyzer SUPERPROBE 73 enabled phase analysis.

The hardness was measured using the Brinell test. The test for the determination of deformation and crack pressure was made on a special equipment, that through the fluid causes the pressure from the inside walls of the pressure dose. The pressure is measured with the manometer. When the dose cracks, the manometer senses the swing at otherwise constant pressure increase. The bottom is under higher load as the walls, so it is thicker and in concave shape. It is necessary that the bottom undergoes under the pressure and goes from concave to convex shape, which is detected as a swing on the manometer. At least 12 bar is demanded for the bottom resistance on the plastic deformation. Furthermore, the crack pressure is detected as a sudden drop of pressure on the manometer. At least 18 bar is demanded for the pressure strength of the pressure dose. The cracks always appear on the upper side of the dose in a longitudinal course because of the texture of the crystal grains.

## Results and Discussion

Chemical analyses of slugs of all three alloys were conducted in the laboratory for quality control of Talum d.d. company and are presented in Table 1.

Computer simulations of thermodynamic equilibrium solidification, equilibrium phase diagram (Figure 3) and equilibrium phase concentration at room temperature were made using Thermo-Calc program for all investigated alloys. For input data the results from the chemical analyses were used (Table 1).

The mass percent of inclusions ($Al_6$(FeMn) and AlMnSi) is with increasing Mn-content which hardens the alloy (Figure 4).

At room temperature, according to the equilibrium calculation, for the 1050 alloy, the primary phase $\alpha_{Al}$ is composed from 99.99 wt. % Al and the phase $Al_6$(FeMn) is composed from 74.47 wt. % Al, 15.50 wt. % Fe and 10.02 wt. %

**Table 1.** Chemical composition of investigated alloys in mass fractions, wt. %

| Alloy | Si | Fe | Mn | Zn | Ti | Rest |
|---|---|---|---|---|---|---|
| **1050** | 0.0913 | 0.2515 | 0.0016 | 0.0089 | 0.0066 | 99.61 |
| **3002** | 0.0726 | 0.2159 | 0.2945 | 0.0085 | 0.0545 | 99.35 |
| **3003** | 0.1917 | 0.5577 | 1.0037 | 0.0087 | 0.0066 | 98.21 |

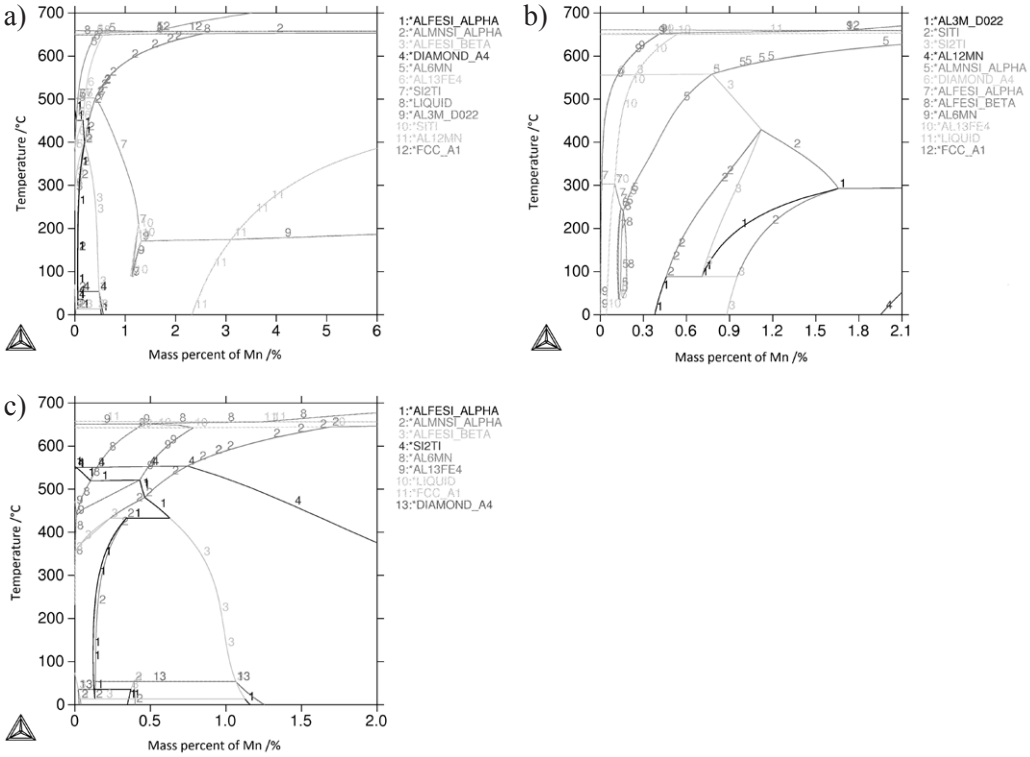


**Figure 3.** Isoplete equilibrium phase diagram of 1050 (a), 3002 (b) and 3003 (c) alloy

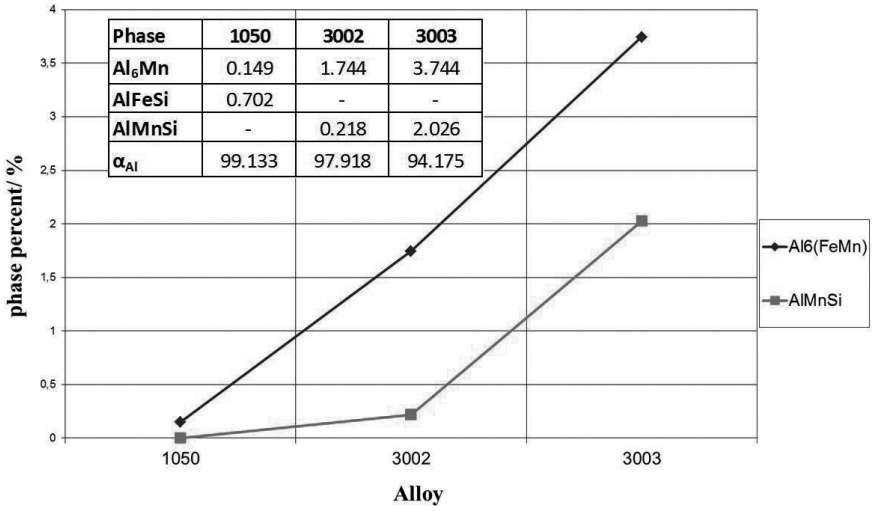


**Figure 4.** Portion of $Al_6$(FeMn) and AlMnSi phase in investigated alloys

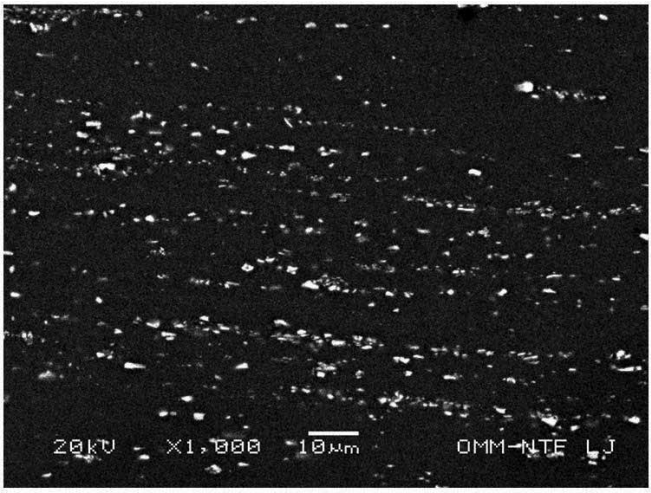


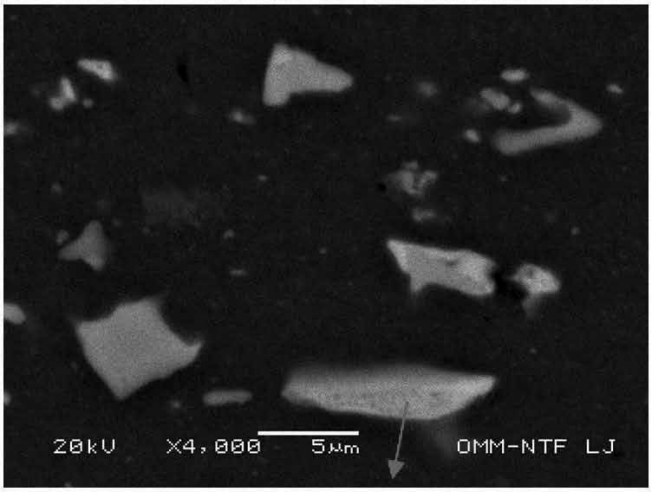


| Elt. | Line | Intensity (c/s) | Error 2-sig | Atomic % | Conc | | |
|---|---|---|---|---|---|---|---|
| Al | Ka | 914.52 | 6.048 | 70.060 | 53.201 | wt.% | |
| Si | Ka | 0.19 | 0.088 | 0.021 | 0.017 | wt.% | |
| Ti | Ka | 2.17 | 0.294 | 0.112 | 0.151 | wt.% | |
| Mn | Ka | 146.24 | 2.419 | 9.944 | 15.375 | wt.% | |
| Fe | Ka | 258.24 | 3.214 | 19.723 | 30.999 | wt.% | |
| Zn | Ka | 0.98 | 0.198 | 0.140 | 0.257 | wt.% | |
| | | | | 100.000 | 100.000 | wt.% | Total |

| | |
|---|---|
| kV | 20.0 |
| Takeoff Angle | 35.0° |
| Elapsed Livetime | 100.0 |

**Figure 5.** Secondary-electron images of specimen C1 in longitudinal course and the inclusions with chemical analysis

Mn. For the 3002 alloy, the primary phase $\alpha_{Al}$ is also composed from 99.99 wt. % Al, $Al_6$(FeMn) phase is composed from 74.51 wt. % Al, 12.38 wt. % Fe and 13.11 wt. % Mn. Phase $\alpha_{Al}$ for the 3003 alloy is composed from 99.99 wt. % Al and phase $Al_6$(FeMn) is composed from 74.48 wt. % Al, 14.90 wt. % Fe and 10.6 wt. % Mn.

**Analyses of inclusions**

Samples C1 (cold forming) and C7 (final product) were examined with scanning electron microscope. In all samples, inclusions $Al_6Mn$ composed of aluminium, iron and manganese were analysed. The inclusions were in longitudinal courses always longitudinal distributed (course of forming) and of polyedric shape (Figure 5).

**Determination of portion and distribution of the inclusions**

Metallographically prepared samples were observed at 500-times magnification (Figure 6), which was most representative for the analysis of the inclusion distribution. The inclusions were distributed at the grain boundaries which were most obviously seen at the unformed specimen with 1 wt. % Mn. The share of the inclusion increases with the increasing of Mn content. So at the input material for 1050 alloy, the surface fraction of the inclusions was 0.8 and for the alloy 3003 1.46 %. After the first stage of the cold forming, the inclusions become smaller and with its position do not indicate anymore the grain crystals, but are distributed along the forming course. Further six steps of forming have no further effect on the amount and distribution of the inclusions.

After microstructure analysis, the portion of the inclusions which appears in the investigated alloys was determined (Table 2). It can be observed that the surface portion of inclusions $Al_6$(FeMn) increases with the increasing of Mn content. Weight portion of inclusions was calculated from the surface portion using the density of $Al_6$(FeMn) inclusions (3.953 g/cm$^3$) which also contain some Fe.

The equilibrium, according to the Thermo-Calc program, shows bigger amount of the phase due to the equilibrium precipitation, which in the praxis is achieved only at a very slow cooling**.** The surface (Table 2) does not capture the whole amount of the inclusions. Phases captured at the analysis of surface portion could be intersected at the various cross-sections, so this can present only the comparison.

**Microstructure analysis of the grains in polarized light**

The samples from the slugs made from 1050, 3002 and 3003 alloys were grinded, polished and electrolytically etched in 5 % HF. From Figure 7 can be seen that at the bigger additions of Mn the crystal grains appear smaller. For the

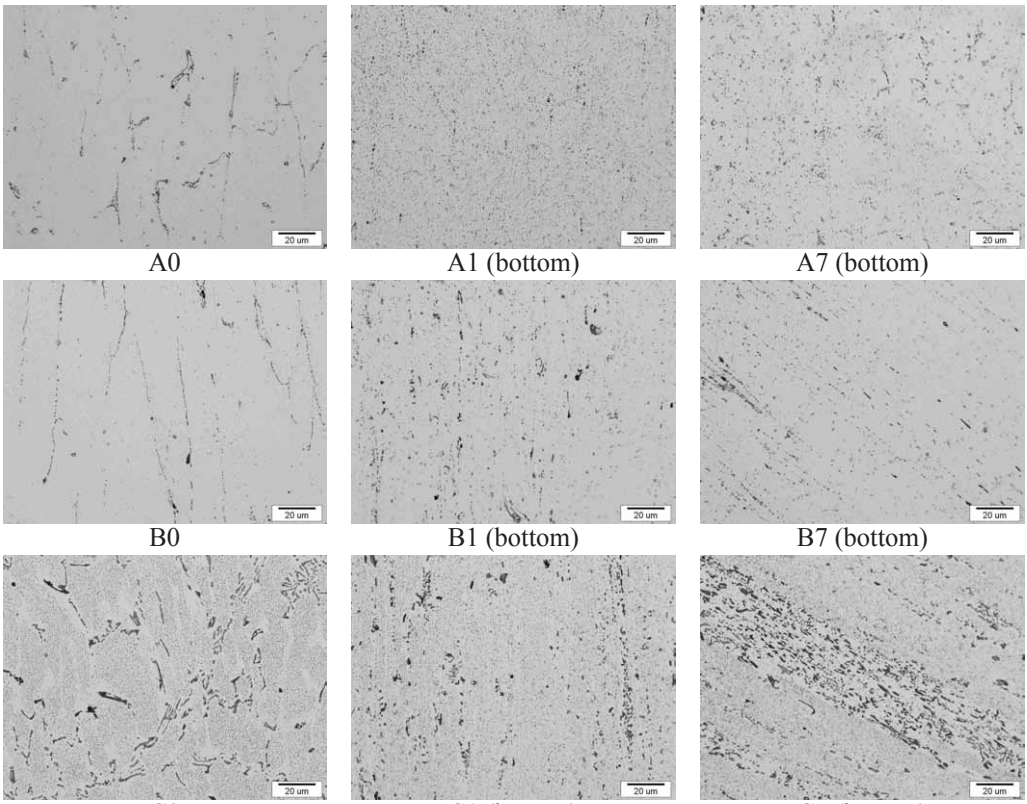


**Figure 6.** Micrographs of analysed samples

**Table 2.** Surface portion of the inclusions in investigated alloys

| Alloy | Surface portion of inclusions | | | Portion of inclusions (wt. %) | | |
|---|---|---|---|---|---|---|
| | (Pos.1) | (Pos.2) | (Pos.3) | (Pos.1) | (Pos.2) | (Pos.3) |
| **1050** | 0.38 | 0.40 | 0.40 | 1.502 | 1.581 | 1.581 |
| **3002** | 0.60 | 0.42 | 0.45 | 2.372 | 1.660 | 1.779 |
| **3002** | 0.84 | 0.56 | 0.56 | 3.321 | 2.214 | 2.214 |

1050 alloy, the grains are 300–600 μm large. For the 3002 alloy, the grains are smaller, only 50–200 μm large and for the 3003 alloy a little bigger, 100–300 μm large. These changes in a grain size could be also consequence of the sampling, how the samples were taken from the slug regarding the impact extrusion respectively. The orientation and the size of the grains could be also a consequence of slug orientation, cut out of casted and formed sheets.

For the samples A1 (after cold forming), A7 (final forming of the pressure dose), C1 and C7 from Figure 8 can be

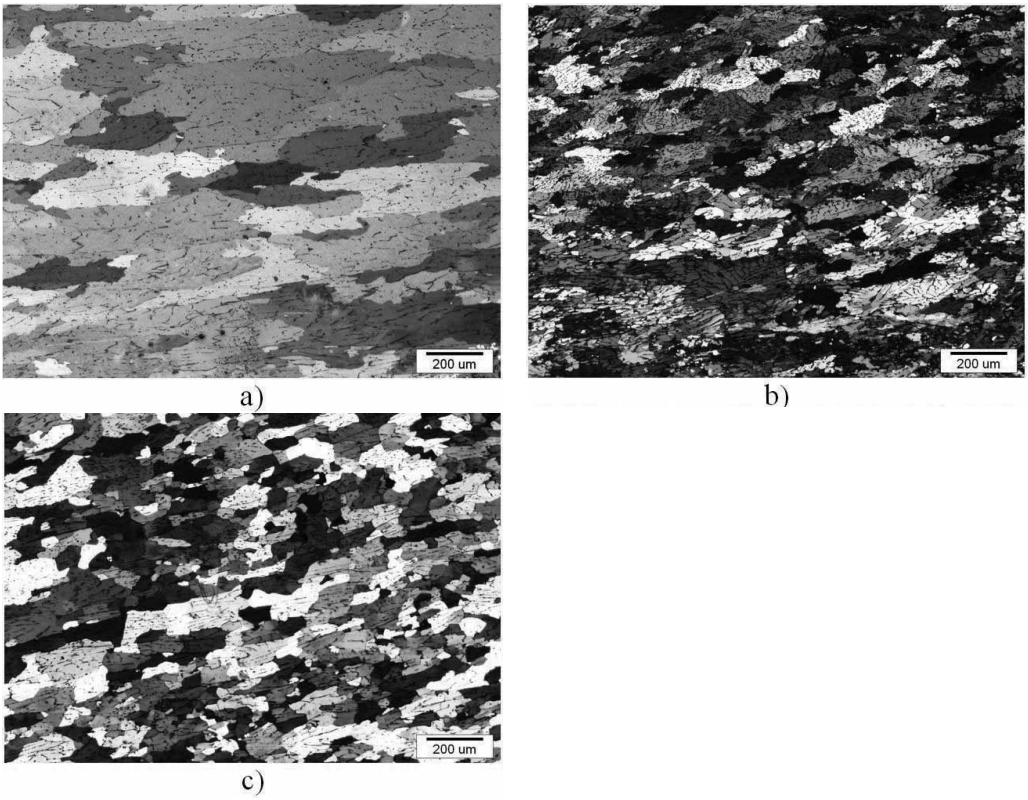


**Figure 7.** Micrographs of crystal grains in the polarized light: 1050 (a), 3002 (b) and 3003 (c) alloy.

observed that at the 200-times magnification, the crystal grains appear elongated (transformed) among which are equally distributed $Al_6(FeMn)$ inclusions. When the samples A and C are compared, the amount of the inclusions in the microstructure increases as the Mn content increases.

The results of Brinell hardness test are presented in Table 3 and the results of the pressure test in Table 4. Mechanical properties, mainly hardness of the input materials, with the increasing of Mn content increase. From Table 4, it is evident that the deformation pressure and crack pressure also increase with the increasing of Mn content in the alloy.

**Table 3.** Hardness of annealed alloys after Brinell

| Alloy | Hardness HB |
|---|---|
| 1050 | 20 |
| 3002 | 22 |
| 3003 | 30 |

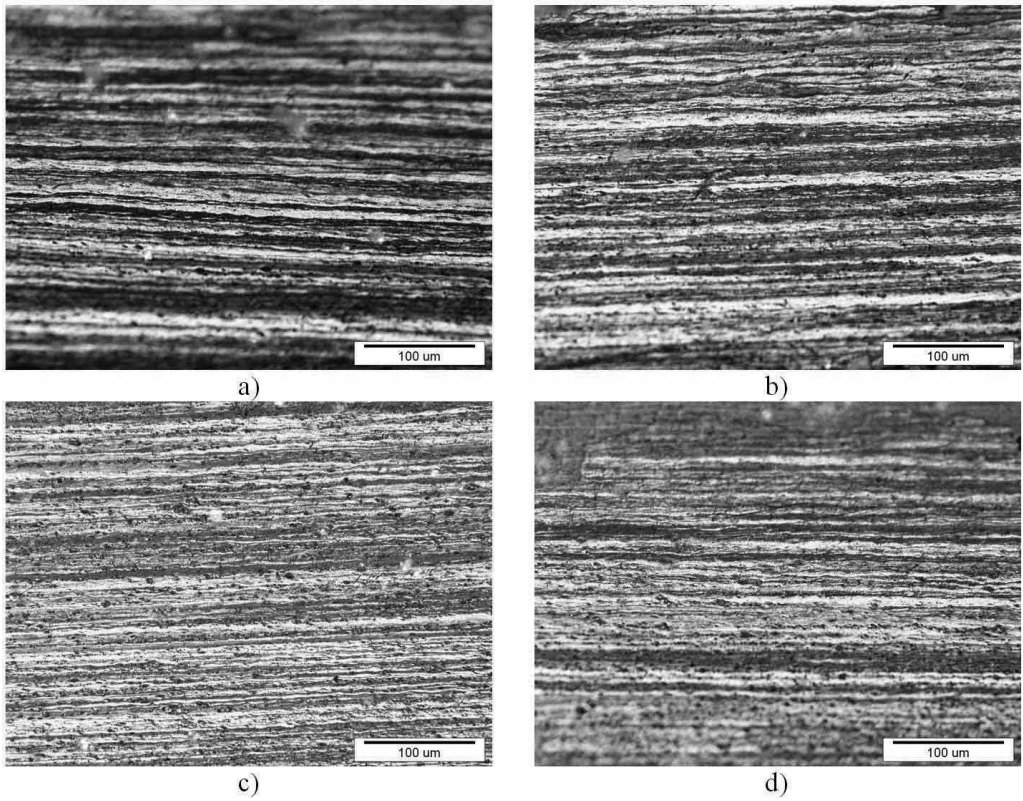


**Figure 8.** Micrographs of samples A1 (a), A7 (b), C1 (c) and C7 (d).

**Table 4.** Results from pressure test

| Alloy | Wahl thickness [mm] | Bottom thickness [mm] | Deformation Pressure [bar] | Cracking pressure [bar] |
|---|---|---|---|---|
| 1050 | 0.4 | 1.1 | 22 | 27 |
| 3002 | 0.4 | 1.1 | 25 | 29 |
| 3003 | 0.4 | 1.1 | 29 | 31 |

## Conclusions

From the mentioned investigations, the following conclusions can be made:
Using the microstructure analysis and computer program Thermo-Calc, the amount of the inclusions in defined alloys was analysed. The amount of the inclusions increases from 0.4 % for the 1050 alloy to 0.45 % for the 3002 alloy and to 0.56 % for the 3003 alloy. According to the calculations with the Thermo-Calc program, the amount of the inclusions that could appear in

these alloys at equilibrium conditions was 0.15 % for the 1050 alloy, 1.74 % for the 3002 alloy and 3.74 % for the 3003 alloy.

The crystal grains of investigated alloys appear elongated (transformed) among which are equally distributed inclusions $Al_6$(FeMn). The concentration of those inclusions is bigger at the edge of the pressure dose and smaller at the middle of the pressure dose. When the specimens A, B and C were compared, it was established that the amount of the inclusions in the microstructure increases as the concentration of Mn in the alloys increases.

In all specimens, the inclusions $Al_6$(FeMn), composed from aluminium, iron and manganese, were analysed. In the longitudinal courses, the inclusions were always longitudinal distributed and of polyedric shape. At the bottom of the pressure dose (sample C9), the inclusions appear in bigger heaps.

The thickness of the bottom and wall of the pressure dose from various alloys is always the same. The deformation pressure was 22 bar for the 1050 alloy and it increases to 25 bar for the 3002 alloy and to 29 bar for the 3003 alloy. The crack pressure also increases when the concentration of Mn increases from 27 bar to 29 bar and finally to 31 bar.

## References

[1] Engler, O. (2012): Control of texture and earing in aluminium alloy AA 3105 sheet for packaging applications, Materials Science and Engineering A, 538, pp. 69–80.

[2] Liu, J., Morris, J. G. (2003): Macro-, micro- and mesotexture evolutions of continuous cast and direct chill cast AA 3105 aluminum alloy during cold rolling, Materials and Engineering A, 357, pp. 277−296.

[3] Liu, W. C., Zhai, T., Morris, J. G. (2004): Texture evolution of continuous cast and direct chill cast AA 3003 aluminum alloys during cold rolling, Scripta Materialia 51, pp. 83–88.

[4] Mondolfo, L. F. (1962): Aluminium alloys: Structure and Properties, Butterworth Co., London.

[5] Martins, J. P., Carvalho, A. L. M., Padilha, A. F. (2009): Microstructure and texture assessment of Al–Mn–Fe–Si (3003) aluminum alloy produced by continuous and semicontinuous casting processes, J Mater Sci 44, pp. 2966–2976.

[6] http://www.talum.si/si/proizvodi/rondelice.php

[7] Liu, W. C., LI, Z., MAN, C. S., RAABE, D., MORRIS, J. G. (2006): Effect of precipitation on rolling texture evolution in continuous cast AA 3105 aluminum alloy, Materials Science and Engineering A, 434, pp. 105–113.

[8] Hatch, J. E. (1990): Aluminum, properties and physical metallurgy, ASM, Metals Park, Ohio.

[9] Li, Y. J., Muggerud, A. M. F., Olsen, A., Furu, T. (2012): Precipitation of partially coherent α-Al(Mn,Fe) Si dispersoids and their strengthening effect in AA 3003 alloy, Acta Materialia, 60, pp. 1004–1014.

[10] Zander, J., Sandstrom, R., Vitos, L. (2007): Modelling mechanical properties for non-hardenable aluminium alloys, Computational Materials Science, 41, pp. 86–95.

[11] Alexander, D. T. L., Greer, A. L. (2002): Solid-state intermetallic phase transformations in 3XXX aluminium alloys, Acta Materialia, 50, pp. 2571–2583.

[12] Li, Y. J., Arnberg, L. (2003): Quantitative study on the precipitation behavior of dispersoids in DC-cast AA3003 alloy during heating and homogenization, Acta Materialia, 51, pp. 3415–3428.

[13] Davis, J. R., Davis & Associates (April 2002): Aluminum and Aluminum Alloys, ASM Specialty handbook, the Materials Information Society, United States of America.